A Fast Edge Detection Model in Presence of Impulse Noise

Yuying Shi[1(✉)], Qian Zhao[1], Feng Guo[1], and Yonggui Zhu[2]

[1] Department of Mathematics and Physics,
North China Electric Power University, Beijing 102206, China
yyshi@amss.ac.cn
[2] School of Science, Communication University of China, Beijing 100024, China

Abstract. Edge detection in image processing is a difficult but meaningful problem. For noisy images, developing fast algorithms with good accuracy and stability is in need. In this work, we propose a variational model which links to the well-known Mumford-Shah functional and design a fast proximity algorithm to solve this new model through a binary labeling processing. Comparing with the famous Ambrosio-Tortorelli model, the efficiency and accuracy of the new model and the proposed minimization algorithm are demonstrated.

Keywords: Mumford-Shah model · Binary level set method · Edge detection · Proximity operator

1 Introduction

Edge detection is important in many scientific fields such as digital image processing, computer vision, material science and physics [2,24], etc. According to the contexts of image processing, edge detection means extracting the boundaries of some objects from a given image. A lot of methods have been proposed for this purpose, such as gradient operator (Roberts operator, Sobel operator, prewitt operator), second-order differential operator (LOG operator, Canny operator) [6] and some new methods (using wavelets, fuzzy algorithms, adaptive splitting (EDAS-1) algorithm [10] etc.). The capability of using gradient operator is limited, as the accuracy of edge identification is usually deteriorated by the presence of noise. Though the second-order differential operator has advantages in denoising and smoothing the edge, it can blur the images which do not have noise. We also notice that the recent researches have favor in using a variety of filter banks to improve the accuracy of edge detection, and the interested readers are referred to [3,10,11,16,22] and the references therein.

Compared with region-based image segmentation, edge detection also focuses on locating open curves belonging to constituent element of edges, yet do not have interior and exterior regional separation. In a recent conference report [25], Wang et al. proposed to embed an open (or a closed) curve into a narrow region (or band), formed by the curve and its parallel curve (also known as the offset

Y.-J. Zhang (Ed.): ICIG 2015, Part I, LNCS 9217, pp. 64–74, 2015.
DOI: 10.1007/978-3-319-21978-3_7

curve [23]). The authors then integrated the Mumford-Shah (MS) model [14] with the binary level-set method, leading to the model dubbed as the modified Mumford-Shah (MMS) model:

$$\min_{u,\psi}\left\{\mu\int_{\Omega}(1-\psi)^2|\nabla u|^2d\boldsymbol{x}+\frac{\nu}{2}\int_{\Omega}(u-I)^2d\boldsymbol{x}+TV(\psi)\right\}. \tag{1}$$

where I is a given image on an open bounded domain $\Omega\subset\mathbb{R}^2$, the minimizer u is expected to be a "good" piecewise smooth approximation of I, μ,ν are positive tuning parameters, and the binary level-set function: $\psi=1$, if $\boldsymbol{x}\in R_d$ (about the concrete definition of R_d, please refer to [20]), while $\psi=0$ otherwise.

Because of the ill-posedness property [5,9] of the above model (1), Shi et al. [20] modified the above model by adding a L_1 regularization term since that the constant function $\psi=1$ and $u=I$ are the solutions of the above model, that is,

$$\min_{u,\psi}\left\{\mu\int_{\Omega}(1-\psi)^2|\nabla u|^2d\boldsymbol{x}+\frac{\nu}{2}\int_{\Omega}(u-I)^2d\boldsymbol{x}+TV(\psi)+\int_{\Omega}|\psi|\,d\boldsymbol{x}\right\}. \tag{2}$$

In another paper, Shi et al. [18] borrowed the idea of [25] and discussed the modified MS model with L^1-norm for impulse noise:

$$\min_{\psi,u}\left\{\mu\int_{\Omega}(1-\psi)^2|\nabla u|^2d\boldsymbol{x}+\frac{\nu}{2}\int_{\Omega}|u-I|d\boldsymbol{x}+TV(\psi)\right\}. \tag{3}$$

The L^1-norm has shown advantages in handling impulse noise such as salt-pepper noise (see, e.g., [7,20]).

Motivated by all the above-mentioned models, here we will show how to solve the following problem for controlling impulse noise:

$$\min_{u,\psi}\left\{\mu\int_{\Omega}(1-\psi)^2|\nabla u|^2d\boldsymbol{x}+\frac{\nu}{2}\int_{\Omega}|u-I|d\boldsymbol{x}+TV(\psi)+\tau\int_{\Omega}|\psi|\,d\boldsymbol{x}\right\}. \tag{4}$$

In fact, the last L^1 norm regularization term $\int_{\Omega}|\psi|\,d\boldsymbol{x}$ tends to favor sparse solution of the edge function ψ [20]. The weight τ is to balance the other terms. By solving the proposed model (4), we can get the restored image u and detected edges simultaneously. Here we will focus on the effect of detected edges.

An auxiliary $q=\psi$ can be used to handle the last term and face the constraint $q=\psi$ by a penalty method. And we let $g=u-I$ as a penalty term, too. So (4) can be approximated by the following unconstrained problem:

$$\begin{aligned}\min_{u,\psi,g,q}\Big\{&\mu\int_{\Omega}(1-\psi)^2|\nabla u|^2d\boldsymbol{x}+\frac{\nu}{2}\int_{\Omega}|g|d\boldsymbol{x}+\frac{\xi}{2}\int_{\Omega}|u-I-g|^2d\boldsymbol{x}\\&+TV(\psi)+\tau\int_{\Omega}|q|\,d\boldsymbol{x}+\frac{r}{2}\int_{\Omega}(q-\psi)^2d\boldsymbol{x}\Big\}.\end{aligned} \tag{5}$$

The rest of the paper is organized as follows. In Sect. 2, for solving the minimization problem, we apply the Proximity algorithm to solve (4). To demonstrate the strengths of the proposed model and the algorithm, we make a comparison with the Ambrosio-Tortorelli model [1] with L^1-norm according to presenting ample numerical results in Sect. 3.

2 The Minimization Algorithm

In this section, we introduce the minimization algorithm for solving (5) and use an iterative method for computing u, and the proximity algorithm for resolving the binary level-set function ψ. We utilize the alternating optimization technique to split (5) into four subproblems:

– u-subproblem: for fixed ψ,g, we solve

$$\min_u \left\{ \Re(u) := \mu \int_\Omega (1-\psi)^2 |\nabla u|^2 d\boldsymbol{x} + \frac{\xi}{2} \int_\Omega |u - I - g|^2 d\boldsymbol{x} \right\}. \tag{6}$$

– ψ-subproblem: for fixed u and q, we solve

$$\min_\psi \left\{ \Im(\psi) := \mu \int_\Omega (1-\psi)^2 |\nabla u|^2 d\boldsymbol{x} + TV(\psi) + \frac{r}{2} \int_\Omega (q-\psi)^2 d\boldsymbol{x} \right\}. \tag{7}$$

– g-subproblem: for fixed u, we solve

$$\min_g \left\{ \frac{\nu}{2} \int_\Omega |g| d\boldsymbol{x} + \frac{\xi}{2} \int_\Omega (u - I - g)^2 d\boldsymbol{x} \right\}. \tag{8}$$

– q-subproblem: for fixed ψ, we solve

$$\min_q \left\{ \tau \int_\Omega |q| d\boldsymbol{x} + \frac{r}{2} \int_\Omega (q-\psi)^2 d\boldsymbol{x} \right\}. \tag{9}$$

We can easily know the solution of (8) can be expressed as

$$g = (u - I) \max \left\{ 0, 1 - \frac{\nu}{2\xi |u - I|} \right\}.$$

Similarly, q can be given

$$q = \psi \max \left\{ 0, 1 - \frac{\tau}{r|\psi|} \right\}.$$

The detailed process can be referred to [19–21]. Next, we present the algorithms for (6) and (7).

2.1 Fixed-Point Iterative Method for Solving u

We first consider (6). Notice that the functional in (6) is convex for fixed ψ, so it admits a unique minimizer. The corresponding Euler-Lagrangian equation takes the form:

$$\begin{cases} -2\mu \mathrm{div}\big((1-\psi)^2 \nabla u\big) + \xi(u - I - g) = 0, \quad \text{in } \Omega, \\ \dfrac{\partial u}{\partial \boldsymbol{n}}\Big|_{\partial\Omega} = 0, \end{cases} \tag{10}$$

where $\boldsymbol{n}$ is the unit outer normal vector to $\partial\Omega$. We expect ψ takes value 0 at the homogeneous region, i.e., $1-\psi \approx 1$. So, we propose to use a fixed-point iterative scheme based on relaxation method to solve this elliptic problem with variable coefficients (see, e.g., [4,15] for similar ideas). We start with the difference equation

$$\begin{aligned}\xi u_{i,j} = 2\mu[&(1-\psi)^2_{i,j+1}(u_{i,j+1}-u_{i,j}) + (1-\psi)^2_{i,j-1}(u_{i,j-1}-u_{i,j})\\ &+ (1-\psi)^2_{i-1,j}(u_{i-1,j}-u_{i,j}) + (1-\psi)^2_{i+1,j}(u_{i+1,j}-u_{i,j})]\\ &+ \xi I_{i,j} + \xi g_{i,j},\end{aligned} \tag{11}$$

where $u_{i,j} \equiv u(i,j)$ is the approximate solution of (10) at grid point (i,j) with grid size $h' = 1$ as usual. Then applying the Gauss-Seidel iteration to (11) leads to

$$\begin{aligned}&\big(2\mu(C_E + C_W + C_N + C_S) + \xi\big)u^{k+1}_{i,j} =\\ &\quad 2\mu\big[C_E u^k_{i,j+1} + C_W u^{k+1}_{i,j-1} + C_N u^{k+1}_{i-1,j} + C_S u^k_{i+1,j}\big] + \xi I_{i,j} + \xi g_{i,j},\end{aligned} \tag{12}$$

where

$$C_E = (1-\psi^k)^2_{i,j+1},\ C_W = (1-\psi^k)^2_{i,j-1},\ C_N = (1-\psi^k)^2_{i-1,j},\ C_S = (1-\psi^k)^2_{i+1,j}.$$

And we implement the relaxation method to speed up the iteration (12). Let

$$u^{k+1}_{i,j} = u^k_{i,j} - \omega_1 r^{k+1}_{i,j}, \tag{13}$$

where $\omega_1 > 0$ is the relaxation factor, and $r^{k+1}_{i,j}$ denotes the residue obtained by subtracting the right-hand side of (12) from the left-hand side of (12). Collecting (13), we have the new scheme:

$$u^{k+1}_{i,j} = \frac{u^k_{i,j} + \omega_1\big(\xi I_{i,j} + \xi g_{i,j} + 2\mu[C_E u^k_{i,j+1} + C_W u^{k+1}_{i,j-1} + C_N u^{k+1}_{i-1,j} + C_S u^k_{i+1,j}]\big)}{1 + \omega_1\big(2\mu(C_E + C_W + C_N + C_S) + \xi\big)}. \tag{14}$$

2.2 Proximity Algorithm for Solving ψ

Now, let us turn to the subproblem (7). Here, we will introduce the proximity method which has been discussed in many papers, and the interested readers are referred to [12,13,20] and the references therein. We begin with a description of notation used in this paper. Let H be a real Hilbert space, and h be a convex functional on H, not identically equal to ∞. The sub-differential of h at $x \in H$ is the set defined by

$$\partial h(x) := \big\{y \in H : h(z) \geq h(x) + \langle y, z-x\rangle,\ \ \forall z \in H\big\},$$

where $\langle\cdot,\cdot\rangle$ is the inner product of H. Then the proximity operator of h at $x \in H$ is defined by

$$\mathrm{prox}_h(x)\ := \arg\min_{u\in H}\left\{\frac{1}{2}\|u-x\|_2^2 + h(u)\right\},$$

where $\|v\|_2 = \sqrt{\langle v, v\rangle}$. The sub-differential and the proximity operator of the function h and $y \in H$ are intimately related. Specifically, for any $x \in H$, we have

$$y \in \partial h(x) \text{ if and only if } x = \text{prox}_h(x + y).$$

To solve the subproblem (7), we define

$$\rho(\psi) = \mu \int_\Omega (1-\psi)^2 |\nabla u|^2 d\boldsymbol{x} + \frac{r}{2} \int_\Omega (q-\psi)^2 d\boldsymbol{x}. \tag{15}$$

Then (7) is equivalent to

$$\min_\psi \big\{ (g \circ B)(\psi) + \rho(\psi) \big\}, \tag{16}$$

where $(g \circ B)(\psi) = TV(\psi)$ and $g(\cdot) = \|\cdot\|_{L^1(\Omega)}, B = \nabla$.

Thus if $\psi \in H(= L^2(\Omega))$ is a solution of (16), then for any $\alpha, \beta > 0$, there exists $\boldsymbol{s} \in H \times H$ such that

$$\psi = \text{prox}_{\frac{1}{\alpha}\rho}\Big(\psi - \frac{\beta}{\alpha} B^* \boldsymbol{s}\Big), \tag{17}$$

and

$$\boldsymbol{s} = (\mathbb{I} - \text{prox}_{\frac{1}{\beta}g})(B\psi + \boldsymbol{s}), \tag{18}$$

where B^* is the adjoint operator of B, and $\mathbb{I}$ is the identity operator.

Conversely, if there exist $\alpha, \beta > 0$, $\boldsymbol{s} \in H \times H$, and $\psi \in H$ satisfying (17) and (18), then ψ is a solution of model (16). So, we have

$$\psi = \text{prox}_{\frac{1}{\alpha}\rho}\Big(\psi - \frac{\beta}{\alpha} B^* \boldsymbol{s}\Big) = \arg\min_{\varpi} \left\{ \frac{1}{\alpha}\rho(\varpi) + \frac{1}{2}\Big\| \varpi - \big(\psi - \frac{\beta}{\alpha} B^* \boldsymbol{s}\big)\Big\|^2_{L^2(\Omega)} \right\}. \tag{19}$$

The corresponding Euler-Lagrangian equation of (19) is:

$$\varpi - M_1 + \frac{1}{\alpha}\big\{ -2\mu(1-\varpi)|\nabla u|^2 + r(\varpi - q)\big\} = 0,$$

where

$$M_1 = \psi - \frac{\beta}{\alpha} B^* \boldsymbol{s}.$$

Equivalently, we get

$$\varpi = \frac{rq + 2\mu|\nabla u|^2 + \alpha M_1}{\alpha + r + 2\mu|\nabla u|^2} \overset{(19)}{=} \psi. \tag{20}$$

Now we will find $\boldsymbol{s}$ in (20) (i.e., in M_1). Equipped with [12], we obtain:

$$\boldsymbol{s} = (B\psi + \boldsymbol{s}) - \max\big\{|B\psi + \boldsymbol{s}| - 1/\beta, 0\big\} \cdot \text{sign}(B\psi + \boldsymbol{s}). \tag{21}$$

That means we solve ψ by the following iteration scheme:

$$\psi^{n+1} = \frac{rq^n + 2\mu|\nabla u^{n+1}|^2 + \alpha\big(\psi^n - \frac{\beta}{\alpha} B^* \boldsymbol{s}^n\big)}{\alpha + r + 2\mu|\nabla u^{n+1}|^2}. \tag{22}$$

After summarizing, we get the Proximity Algorithm for (5).

Proximity Algorithm

1. Initialization: set $\boldsymbol{s}^0 = \mathbf{0}$, and input ψ^0, u^0, $g^0, \mu, \nu, \xi, \alpha, \beta, \omega_1, r, \tau$.
2. For $n = 0, 1, \cdots$,
   (i) Update u^{n+1} using the iteration scheme (14) with initial value u^n and ψ^n (in place of ψ);
   (ii) Update q^n by
$$q^n = \psi^n \max\Big\{0, 1 - \frac{\tau}{r|\psi^n|}\Big\}.$$
   (iii) Update g^n by
$$g^n = (u - I)^n \max\Big\{0, 1 - \frac{\nu}{2\xi|(u - I)^n|}\Big\}.$$
   (iv) Update ψ^{n+1} using the iteration scheme (22).
   (v) Update $\boldsymbol{s}^{n+1}$ by
$$\boldsymbol{s}^{n+1} = (B\psi^{n+1} + \boldsymbol{s}^n) - \max\big\{|B\psi^{n+1} + \boldsymbol{s}^n| - 1/\beta, 0\big\} \cdot \operatorname{sign}(B\psi^{n+1} + \boldsymbol{s}^n).$$
3. Endfor till some stopping rule meets.

As with the previous algorithm, the iteration in Step 2 (i) can be ran for several times. Huang et al. [8] showed that the alternating direction method (ADM) with exactly solving inner subproblems enjoys a linear convergence in the context of variational image restoration. As with [20], such a convergence theorem can be observed for our new model (5). The only difference is the substitution of $I_{i,j} + g_{i,j}$ for $I_{i,j}$ in the progress of proof.

Theorem 1. *The sequence* $\{u^k\}_{k\geqslant 0}$ *(resp.* $\{\psi^k\}_{k\geqslant 0}$*) generated by the inner iterative scheme* (14)*(resp.* (22)*) converges to the solution of the problem* (6) *(resp.* (7)*).*

Theorem 2. *Let* (u^*, ψ^*) *be the pair of minimizers of the subproblems* (6)-(7)*. Given* ω_1 *in the Proximity algorithm, we have*

$$\lim_{n\to+\infty} \Im(\psi^n) = \Im(\psi^*), \quad \lim_{n\to+\infty} \Re(u^n) = \Re(u^*).$$

Moreover, if the pair of minimizers is unique, we get

$$\lim_{n\to+\infty} \|\psi^n - \psi^*\| = 0, \quad \lim_{n\to+\infty} \|u^n - u^*\| = 0.$$

3 Numerical Experiments

In this section, we present the new AT model equipped with L^1-norm and provide ample numerical results to compare the relevant two algorithms.

3.1 Algorithm for Ambrosio and Tortorelli Model

We first give the AT model with L^1-norm as the fidelity term:

$$E_{AT}(u,v)=\mu\int_{\Omega}(v^2+o_{\varepsilon})|\nabla u|^2d\boldsymbol{x}+\frac{\nu}{2}\int_{\Omega}|u-I|d\boldsymbol{x}+\int_{\Omega}\Big(\varepsilon|\nabla v|^2+\frac{1}{4\varepsilon}(v-1)^2\Big)d\boldsymbol{x}, \tag{23}$$

where ε is a sufficient small parameter, and o_{ε} is any non-negative infinitesimal quantity approaching 0 faster than ε. Shah [17] considered replacing the first term of the above model (23) with L^1-functions.

Similarly, we set $g=u-I$ by a penalty method. Then equation (23) can be approximated as follows:

$$\begin{aligned}E_{AT}(u,v,g)=&\mu\int_{\Omega}(v^2+o_{\varepsilon})|\nabla u|^2d\boldsymbol{x}+\frac{\nu}{2}\int_{\Omega}|g|d\boldsymbol{x}\\&+\frac{\xi}{2}\int_{\Omega}|u-I-g|^2d\boldsymbol{x}+\int_{\Omega}\Big(\varepsilon|\nabla v|^2+\frac{1}{4\varepsilon}(v-1)^2\Big)d\boldsymbol{x},\end{aligned} \tag{24}$$

As mentioned like foregoing, we need to solve the following subproblems of the AT model (24) :

$$\begin{cases}u=\dfrac{2\mu}{\xi}\mathrm{div}\big[(v^2+o_{\epsilon})\nabla u\big]+I+g, & \text{in } \Omega,\\ v\Big(\dfrac{1}{4\epsilon}+\mu|\nabla u|^2\Big)=\epsilon\Delta v+\dfrac{1}{4\epsilon}, & \text{in } \Omega,\\ g=arg\min\limits_{g}\dfrac{\nu}{2}\displaystyle\int_{\Omega}|g|d\boldsymbol{x}+\frac{\xi}{2}\int_{\Omega}|u-I-g|^2d\boldsymbol{x}, & \text{in } \Omega,\\ \dfrac{\partial u}{\partial\boldsymbol{n}}=\dfrac{\partial v}{\partial\boldsymbol{n}}=0, & \text{on } \partial\Omega.\end{cases} \tag{25}$$

We solve u by the iterative scheme:

$$u_{i,j}^{n+1}=\frac{u_{i,j}^{n}+\omega_3\big(\xi I_{i,j}+\xi g_{i,j}+2\mu[C_E u_{i,j+1}^{n}+C_W u_{i,j-1}^{n+1}+C_N u_{i-1,j}^{n+1}+C_S u_{i+1,j}^{n}]\big)}{1+\omega_3\big(2\mu(C_E+C_W+C_N+C_S)+\xi\big)}, \tag{26}$$

where $\omega_3>0$ is the relaxation factor and

$$C_E=(v^n)_{i,j+1}^2+o_{\epsilon},C_W=(v^n)_{i,j-1}^2+o_{\epsilon},C_N=(v^n)_{i-1,j}^2+o_{\epsilon},C_S=(v^n)_{i+1,j}^2+o_{\epsilon}.$$

We solve v by the fixed-point iteration:

$$v_{i,j}^{n+1}=\frac{v_{i,j}^{n}+\omega_4\big(\frac{1}{4\epsilon}+\epsilon(v_{i+1,j}^{n}+v_{i-1,j}^{n+1}+v_{i,j-1}^{n+1}+v_{i,j+1}^{n})\big)}{1+\omega_4(\frac{1}{4\epsilon}+2\mu|\nabla u_{i,j}^{n+1}|^2+4\epsilon)}, \tag{27}$$

where $\omega_4>0$ is the relaxation factor. And for fixed u, g can be given

$$g=(u-I)\max\Big\{0,1-\frac{\nu}{2\xi|u-I|}\Big\}. \tag{28}$$

Now, we present the full algorithm as follows.

AT Algorithm

1. Initialization: set $o_\epsilon = \epsilon^{\hat{p}}(\hat{p} > 1)$, and input u^0, v^0, g^0, μ, ν, ξ, $\hat{p}$, ϵ, ω_3, ω_4.
2. For $n = 0, 1, \cdots$,
   (i) Update u^{n+1} by (26);
   (ii) Update v^{n+1} by (27).
   (iii) Update g^{n+1} by (28).
3. Endfor till some stopping rule meets.

3.2 Comparisons

Next, we compare the following two algorithms: the AT algorithm stated above and the Proximity algorithm. Here, we set the stopping rule by using the relative error

$$E(u^{n+1}, u^n) := \|u^{n+1} - u^n\|^2 \leq \eta, \tag{29}$$

where a prescribed tolerance $\eta > 0$. The choice of the parameters are specified in the captions of the figures.

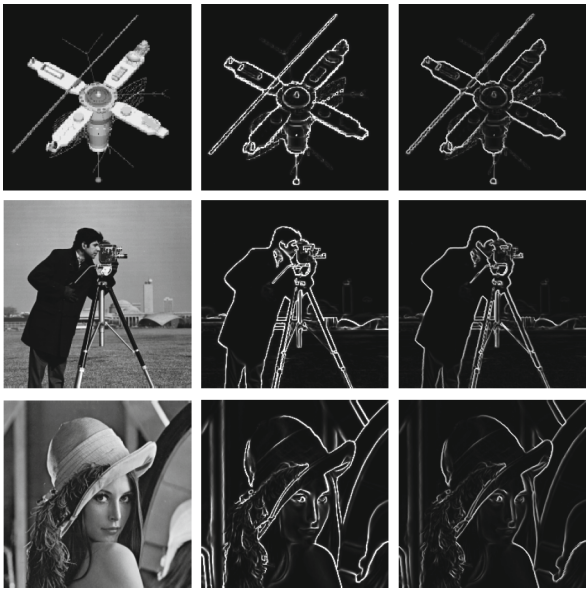

Fig. 1. Column 1: Original images; Column 2: edges detected by the Proximity algorithm; Column 3: edges detected by the AT algorithm.

Fig. 2. Column 1: Noisy images contaminated by salt and pepper noise with $\sigma = 0.04$; Column 2: edges detected by the Poximity algorithm; Column 3: edges detected by the AT algorithm.

In the first experiment, we test three real clean images (see Fig. 1), and generally choose the same parameters in the Proximity algorithm and the AT algorithm with

$$\mu = 3 \times 10^4, \nu = 1, \omega_1 = 5 \times 10^{-4}, r = 3 \times 10^4, \eta = 1 \times 10^{-6}, \xi = 5 \times 10^3$$

and $\alpha = 0.01, \beta = 0.01, \tau = 1$ in the Proximity algorithm and $\epsilon = 0.01, \hat{p} = 2$ in the AT algorithm, respectively. Shi [20] showed the robustness of the parameters for the model there. Here, we have tested many parameters for different images, our model also keeps the robustness property. We present three original images and the edges detected by the above two different algorithms in Fig. 1. From the figures, we observe that our new model (5) outperforms the AT model. Because the proposed Proximity algorithm can detect all the meaningful edges, and the edges are more continuous and clear than the AT model.

In the second experiment, we turn to the comparison of the above two algorithms for the noisy images in Fig. 2 (salt-pepper noise with $\sigma = 0.04$). In this situation, solving u equation usually not only need one iteration in order to smooth the noisy image. We choose $\xi = 1.5 \times 10^3$, and other parameters are the same as the previous examples. Figure 2 shows the noisy images and the detected results obtained by the two different algorithms. Obviously, our new model using the Proximity algorithm yields more meaningful edges, but the AT model smoothes some details of the edges. Different types of noise will be discussed in the following paper.

Acknowledgments. This research is supported by NSFC (No. 11271126) and the Fundamental Research Funds for the Central Universities (No. 2014ZZD10).

References

1. Ambrosio, L., Tortorelli, V.: Approximation of functions depending on jumps by elliptic functions via Γ-convergence. Comm. Pure Appl. Math. **13**, 999–1036 (1990)
2. Berkels, B., Rätz, A., Rumpf, M., Voigt, A.: Extracting grain boundaries and macroscopic deformations from images on atomic scale. J. Sci. Comput. **35**(1), 1–23 (2008)
3. Brook, A., Kimmel, R., Sochen, N.: Variational restoration and edge detection for color images. J. Math. Imaging Vis. **18**(3), 247–268 (2003)
4. Chambolle, A.: An algorithm for total variation minimization and applications. J. Math. Imaging Vis. **20**(1–2), 89–97 (2004)
5. Chan, T., Esedoglu, S., Nikolova, M.: Algorithms for finding global minimizers of image segmentation and denoising models. SIAM J. Appl. Math. **66**(5), 1632–1648 (2006)
6. Chan, T., Shen, J.: Image processing and Analysis. Society for Industrial and Applied Mathematics (SIAM), Philadelphia, PA, Variational, PDE, Wavelet, and Stochastic Methods (2005)
7. Goldstein, T., Osher, S.: The split Bregman method for L1 regularized problems. SIAM J. Imaging Sci. **2**(2), 323–343 (2009)
8. Huang, Y., Lu, D., Zeng, T.: Two-step approach for the restoration of images corrupted by multiplicative noise. SIAM J. Sci. Comput. **35**(6), A2856–A2873 (2013)
9. S. Lee, H. Lee, P. Abbeel, and A. Ng. Efficient l_1 regularized logistic regression. In Proceedings of the National Conference on Artificial Intelligence, volume 21, pages 401–408. MIT Press, 2011
10. Llanas, B., Lantarón, S.: Edge detection by adaptive splitting. J. Sci. Comput. **46**(3), 486–518 (2011)
11. Meinhardt, E., Zacur, E., Frangi, A., Caselles, V.: 3D edge detection by selection of level surface patches. J. Math. Imaging Vis. **34**(1), 1–16 (2009)
12. Micchelli, C., Shen, L., Xu, Y.: Proximity algorithms for image models: denoising. Inverse Probl. **27**(4), 045009 (2011)
13. J. Moreau. Fonctions convexes duales et points proximaux dans un espace hilbertien. C.R. Acad. Sci. Paris Sér. A Math., 255:1897–2899, 1962
14. Mumford, D., Shah, J.: Optimal approximations by piecewise smooth functions and associated variational problems. Comm. Pure Appl. Math. **42**(5), 577–685 (1989)
15. Perona, P., Malik, J.: Scale-space and edge-detection using anisotropic diffusion. IEEE T. Pattern Anal. **12**(7), 629–639 (1990)
16. T. Pock, D. Cremers, H. Bischof, and A. Chambolle. An algorithm for minimizing the Mumford-Shah functional. In Computer Vision, 12th International Conference on, pages 1133–1140. IEEE, 2009
17. J. Shah. A common framework for curve evolution, segmentation and anisotropic diffusion. IEEE Conference on Computer Vision and Pattern Recognition, pages 136–142, 1996
18. Shi, Y., Guo, F., Su, X., Xu, J.: Edge Detection in Presence of Impulse Noise. In: Tan, T., Ruan, Q., Wang, S., Ma, H., Huang, K. (eds.) IGTA 2014. CCIS, vol. 437, pp. 8–18. Springer, Heidelberg (2014)
19. Shi, Y., Wang, L., Tai, X.: Geometry of total variation regularized Lp-model. J. Comput. Appl. Math. **236**(8), 2223–2234 (2012)

20. Shi, Y., Ying, G., Wang, L., Tai, X.: A fast edge detection algorithm using binary labels. Inverse Probl. Imag. **9**(2), 551–578 (2015)
21. Tai, X., Wu, C.: Augmented Lagrangian method, dual methods and split Bregman iteration for ROF model. In: Scale Space and Variational Methods in Computer Vision, Proceedings, vol. 5567 of Lecture Notes in Computer Science, pp. 502–513. Elsevier (2009)
22. Tao, W., Chang, F., Liu, L., Jin, H., Wang, T.: Interactively multiphase image segmentation based on variational formulation and graph cuts. Pattern Recogn. **43**(10), 3208–3218 (2010)
23. Toponogov, V.: Differential Geometry of Curves and Surfaces: A Concise Guide. Birkhauser Verlag, Basel (2006)
24. Upmanyu, M., Smith, R., Srolovitz, D.: Atomistic simulation of curvature driven grain boundary migration. Interface Sci. **6**, 41–58 (1998)
25. Wang, L.-L., Shi, Y., Tai, X.-C.: Robust edge detection using Mumford-Shah model and binary level set method. In: Bruckstein, A.M., ter Haar Romeny, B.M., Bronstein, A.M., Bronstein, M.M. (eds.) SSVM 2011. LNCS, vol. 6667, pp. 291–301. Springer, Heidelberg (2012)